

## Nuclear Enhancement of $\pi^0$ and $\eta$ Mesons Produced at Large Transverse Momenta

J. Povlis, J. Biel, C. Bromberg, B. Brown, C. Chandlee, S. Cihangir, S. R. W. Cooper, T. Ferbel, D. Garelick, G. Glass,<sup>(a)</sup> M. Glaubman, S.-R. Han,<sup>(b)</sup> K. Heller, S. Hossain, J. Huston, A. Jonckheere, J. LeBritton,<sup>(c)</sup> R. A. Lewis,<sup>(d)</sup> F. Lobkowicz, M. McLaughlin, M. Marshak, C. A. Nelson, Jr., E. Peterson, E. Pothier, K. Ruddick, M. Shupe, P. Slattery, and G. A. Smith<sup>(d)</sup>

*Fermilab, Batavia, Illinois 60510, and Michigan State University, East Lansing, Michigan 48824, and University of Minnesota, Minneapolis, Minnesota 55455, and Northeastern University, Boston, Massachusetts 02115, and University of Rochester, Rochester, New York 14627*

(Received 10 May 1983)

The authors have measured the large- $p_T$  inclusive cross sections for  $\pi^0$  and  $\eta$  production near  $90^\circ$  in the center-of-mass system in 200-GeV/c  $\pi^+$  and proton collisions with beryllium, carbon, and aluminum targets. The cross section for both  $\pi^0$  and  $\eta$  mesons rises with increasing nucleon number ( $A$ ) of the target nucleus as  $A^\alpha$ , with  $\alpha > 1$ . The ratio of the  $\pi^0$  yield in  $pA$  collisions to that in  $\pi^+A$  collisions decreases with increasing  $p_T$ .

PACS numbers: 13.85.Ni

It has been known for some time that hadron-nucleus inelastic total cross sections increase nearly in proportion to  $A^{2/3}$ . This suggests that strong interactions at the surface of the nucleus shield the interior from the incident beam. On the other hand, single-particle production on nuclear targets at large transverse momenta has been found to increase in proportion to  $A^\alpha$ , with values of  $\alpha > 1$ .<sup>1</sup> Although secondary scattering mechanisms can account for the anomalous nuclear enhancement,<sup>2</sup> there is as yet no generally accepted explanation for the effect. It has been suggested that the dependence of the power  $\alpha$  on the species of produced particles might be sensitive to the dynamics. Previous measurements of  $\alpha$  at large  $p_T$  range from  $\sim 1.1$  for producing  $\pi^\pm$  to  $\sim 1.3$  for producing protons.<sup>1</sup> Here we report on an experiment performed in the M-1 beam at Fermilab, which extends such measurements to include neutral mesons.

The overall arrangement for the experiment is shown in Nelson *et al.*<sup>3</sup> The incident positive beam (83%  $p$ , 3%  $K^+$ , 14%  $\pi^+$ ) of 200 GeV/c momentum was defined by several scintillation counters. A Cherenkov counter in the beam line was used to tag  $\pi^+$  particles (kaons were treated as protons). The nuclear targets were  $\sim 0.1$  radiation length thick. Two sets of counters downstream of the target, situated just outside of the beam, were used to define an interaction in the target. Various veto and halo counters suppressed triggers from the region around the beam; also, a wall of scintillation counters, that shadowed our electromagnetic-shower detector, suppressed triggers from particles produced by interactions upstream of the target.

Photons were detected using a liquid-argon calorimeter (LAC), located 8 m from the target, and centered at an angle of 100 mrad relative to the beam; at large  $p_T$ , this angle corresponds to a production angle of  $90^\circ$  in the center-of-mass system for this experiment. The sensitive area of the LAC was 1.4 m  $\times$  0.81 m. The LAC had alternate layers of X and Y readout strips; the strips were 1.27 cm wide. The correlation between the X and Y view was made on the basis of energy matching. Further details on the LAC construction and performance are given in Ref. 3.

The trigger for the experiment required an interaction signal from counters just downstream of the target and a suitably large transverse momentum signal from the LAC. A "global  $p_T$ " signal was formed with specialized electronics that added all of the 112 X-strip energies, each attenuated by a factor equal to  $\sin\theta$  for that strip, where  $\theta$  is the laboratory angle; i.e.,  $(p_T)_{\text{global}} = \sum_{i=1}^{112} E_i \sin\theta_i$ . The trigger threshold was adjusted in order to equalize the data accumulation rate across the detector. The effective threshold varied from  $p_T \sim 2.3$  GeV/c at large angles to  $p_T \sim 3.0$  GeV/c at small angles. The trigger reached nearly full efficiency  $\sim 0.5$  GeV/c above the nominal threshold value. We will present our results corrected for this inefficiency.

In addition to the global- $p_T$  trigger, a "local  $p_T$ " requirement of at least 0.6 GeV/c in three neighboring X strips was also imposed at the trigger level. This served to suppress coherent noise and those multiphoton events in which there were no  $\pi^0$  or  $\eta$  mesons produced with  $p_T$  above 1.2 GeV/c.

A minimum energy cut of 1 GeV per photon

yielded an average photon multiplicity for all triggers of 4.4 photons in the LAC per event. When at least one two-photon combination had a  $p_T > 2.5$  GeV/c, this multiplicity dropped to 2.6 photons per event.

In Fig. 1 we show the two-photon mass spectra for all photon pairs with  $p_T > 2.1$  GeV/c, and energy asymmetry  $A < 0.8$ , where  $A = |E_{\gamma_1} - E_{\gamma_2}| / (E_{\gamma_1} + E_{\gamma_2}) = |\cos \theta_H|$ , with  $\theta_H$  the helicity angle of the photon in  $\pi^0$  or  $\eta$  decay. A narrow signal above a very small background is seen at the  $\pi^0$  mass, and a clear signal is observed at the  $\eta$  mass. Reconstruction efficiencies for  $\pi^0$  and  $\eta$  events are greater than 99% for two-photon events, and are on the average  $\sim 95\%$  for photon multiplicities above two. For further analysis, the  $\pi^0$  and  $\eta$  mass regions were defined, respectively, by a 50-MeV band centered on the  $\pi^0$  mass, and a 100-MeV band centered on the observed  $\eta$  mass. In extracting cross sections as a function of  $p_T$ , a sideband subtraction of the background was performed and normalized according to the fits shown in Fig. 1.<sup>4</sup>

A Monte Carlo simulation of the detector was used to evaluate the geometrical and trigger efficiencies of each observed event. For  $\pi^0$ 's pointing from the target to a fiducial area of 110 cm

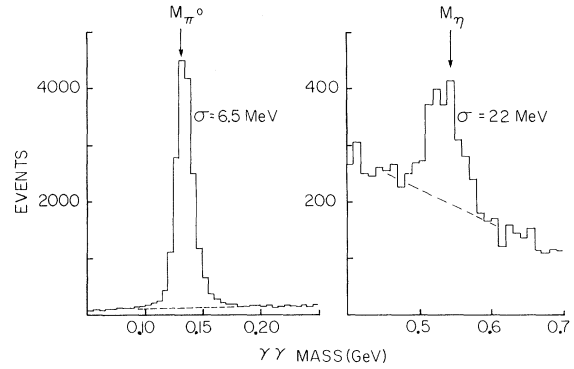


FIG. 1. Two-photon mass spectra for photon pairs with energy asymmetry  $A < 0.8$ .

in  $X$  by 60 cm in  $Y$  the geometrical efficiency for  $|\cos \theta_H| < 0.8$  was typically  $\sim 90\%$ ; the worst overall efficiency (trigger and geometry combined) was  $\sim 30\%$  near the very edges of the fiducial region. In the results to be presented, only statistical uncertainties will be given. Systematic uncertainties in the  $p_T$  scale arise from two main sources: namely, survey uncertainties in the position of the LAC (1%), and uncertainties in the energy calibration ( $\sim 1.5\%$ ). We estimated the latter through our ability to constrain simulta-

TABLE I. Invariant cross sections for  $\pi^0$  production ( $\text{cm}^2/\text{GeV}^2$  nucleus) averaged over the  $p_T$  bin and the center-of-mass rapidity interval ( $-0.75$  to  $+0.2$ ).

$p_T$ (GeV/c)	pBe	$\pi^+$ Be	pC	$\pi^+$ C	pAl	$\pi^+$ Al
2.15	$1.03 \pm 0.11 \times 10^{-29}$	$8.4 \pm 2.6 \times 10^{-30}$	$1.47 \pm 0.04 \times 10^{-29}$	$1.19 \pm 0.11 \times 10^{-29}$	$3.51 \pm 0.32 \times 10^{-29}$	$2.94 \pm 0.87 \times 10^{-29}$
2.25	$7.47 \pm 0.83 \times 10^{-30}$	$7.4 \pm 2.3 \times 10^{-30}$	$1.07 \pm 0.03 \times 10^{-29}$	$7.88 \pm 0.90 \times 10^{-30}$	$2.55 \pm 0.24 \times 10^{-29}$	$1.89 \pm 0.69 \times 10^{-29}$
2.35	$6.04 \pm 0.49 \times 10^{-30}$	$6.9 \pm 1.6 \times 10^{-30}$	$7.13 \pm 0.19 \times 10^{-30}$	$4.93 \pm 0.47 \times 10^{-30}$	$1.81 \pm 0.14 \times 10^{-29}$	$1.52 \pm 0.36 \times 10^{-29}$
2.45	$3.71 \pm 0.36 \times 10^{-30}$	$3.0 \pm 0.9 \times 10^{-30}$	$4.57 \pm 0.13 \times 10^{-30}$	$3.83 \pm 0.35 \times 10^{-30}$	$1.12 \pm 0.10 \times 10^{-29}$	$1.04 \pm 0.30 \times 10^{-29}$
2.55	$2.41 \pm 0.27 \times 10^{-30}$	$1.9 \pm 0.8 \times 10^{-30}$	$2.95 \pm 0.10 \times 10^{-30}$	$2.79 \pm 0.29 \times 10^{-30}$	$8.66 \pm 0.78 \times 10^{-30}$	$9.5 \pm 2.3 \times 10^{-30}$
2.65	$1.73 \pm 0.18 \times 10^{-30}$	$1.1 \pm 0.4 \times 10^{-30}$	$2.02 \pm 0.07 \times 10^{-30}$	$2.14 \pm 0.19 \times 10^{-30}$	$5.75 \pm 0.51 \times 10^{-30}$	$4.1 \pm 1.6 \times 10^{-30}$
2.75	$8.68 \pm 1.12 \times 10^{-31}$	$1.2 \pm 0.3 \times 10^{-30}$	$1.30 \pm 0.05 \times 10^{-30}$	$1.10 \pm 0.14 \times 10^{-30}$	$3.79 \pm 0.39 \times 10^{-30}$	$3.7 \pm 1.0 \times 10^{-30}$
2.85	$7.48 \pm 0.97 \times 10^{-31}$	$8.4 \pm 2.9 \times 10^{-31}$	$8.56 \pm 0.38 \times 10^{-31}$	$9.6 \pm 1.1 \times 10^{-31}$	$2.14 \pm 0.28 \times 10^{-30}$	$2.5 \pm 0.9 \times 10^{-30}$
2.95	$3.92 \pm 0.64 \times 10^{-31}$	$5.0 \pm 2.0 \times 10^{-31}$	$6.22 \pm 0.31 \times 10^{-31}$	$6.0 \pm 0.9 \times 10^{-31}$	$1.53 \pm 0.23 \times 10^{-30}$	$1.6 \pm 0.6 \times 10^{-30}$
3.10	$2.51 \pm 0.37 \times 10^{-31}$	$4.2 \pm 1.3 \times 10^{-31}$	$3.57 \pm 0.16 \times 10^{-31}$	$3.3 \pm 0.5 \times 10^{-31}$	$8.0 \pm 1.1 \times 10^{-31}$	$8.3 \pm 3.1 \times 10^{-31}$
3.30	$9.6 \pm 2.1 \times 10^{-32}$	$1.6 \pm 0.7 \times 10^{-31}$	$1.64 \pm 0.10 \times 10^{-31}$	$1.8 \pm 0.3 \times 10^{-31}$	$3.9 \pm 0.7 \times 10^{-31}$	$9.5 \pm 3.0 \times 10^{-31}$
3.50	$6.7 \pm 1.7 \times 10^{-32}$	$6.8 \pm 5.9 \times 10^{-32}$	$7.23 \pm 0.67 \times 10^{-32}$	$1.0 \pm 0.2 \times 10^{-31}$	$2.7 \pm 0.6 \times 10^{-31}$	$1.8 \pm 1.3 \times 10^{-31}$
3.80	$2.1 \pm 0.6 \times 10^{-32}$	$3.8 \pm 2.6 \times 10^{-32}$	$2.56 \pm 0.25 \times 10^{-32}$	$1.7 \pm 0.7 \times 10^{-32}$	$9.8 \pm 2.4 \times 10^{-32}$	$1.8 \pm 0.8 \times 10^{-31}$
4.25			$5.5 \pm 1.0 \times 10^{-33}$	$4.8 \pm 2.2 \times 10^{-33}$	$1.3 \pm 0.9 \times 10^{-32}$	
4.75			$1.0 \pm 0.4 \times 10^{-33}$			

TABLE II. Invariant cross sections for  $\eta$  production ( $\text{cm}^2/\text{GeV}^2$  nucleus) averaged over the  $p_T$  bin and the center-of-mass rapidity interval ( $-0.5$  to  $+0.1$ ).

$p_T$ (GeV/c)	pBe	pC	$\pi^+C$	pAl
2.40	$2.1 \pm 0.8 \times 10^{-30}$	$2.9 \pm 0.3 \times 10^{-30}$	$2.9 \pm 1.0 \times 10^{-30}$	$7.4 \pm 2.4 \times 10^{-30}$
2.60	$4.1 \pm 3.4 \times 10^{-31}$	$1.2 \pm 0.2 \times 10^{-30}$	$4.8 \pm 3.7 \times 10^{-31}$	$2.3 \pm 1.0 \times 10^{-30}$
2.85	$1.5 \pm 1.2 \times 10^{-31}$	$4.9 \pm 0.6 \times 10^{-31}$	$3.8 \pm 1.7 \times 10^{-31}$	$1.2 \pm 0.5 \times 10^{-30}$
3.20	$6.4 \pm 4.3 \times 10^{-32}$	$1.5 \pm 0.2 \times 10^{-31}$	$1.3 \pm 0.6 \times 10^{-31}$	
3.70	$3.4 \pm 1.8 \times 10^{-32}$	$2.6 \pm 0.7 \times 10^{-32}$		
4.50		$1.2 \pm 1.1 \times 10^{-33}$		

neously the  $\pi^0$  and  $\eta$  masses to within  $\sim 1\%$  of accepted values. The effects of changes in the  $p_T$  scale, combined with other uncertainties, yield an absolute normalization uncertainty of  $\pm 15\%$  in our cross sections.

The cross sections for  $\pi^0$  and  $\eta$  production are given, respectively, in Table I and Table II. The proton data are displayed in Fig. 2. We have fitted the nuclear-target dependence of the cross sections by the commonly used form  $A^\alpha$ , which adequately describes our data. The fit yields a value of  $\alpha_{\pi^0} = 1.11 \pm 0.05$  for  $pA \rightarrow \pi^0 X$ . (We have not observed a significant variation of

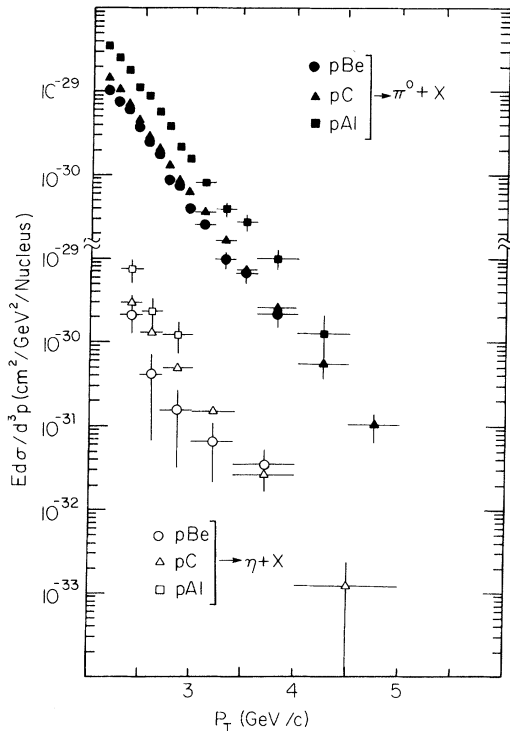


FIG. 2. Invariant cross sections for the production of  $\pi^0$  and  $\eta$  in proton-nucleus collisions at 200 GeV/c.

$\alpha$  with  $p_T$  or rapidity and have consequently integrated over our  $p_T$  and rapidity ranges.) We have also obtained fitted values of  $\alpha_\eta = 1.14 \pm 0.30$  for  $pA \rightarrow \eta X$  and  $\alpha_{\pi^0} = 1.11 \pm 0.15$  for  $\pi^+A \rightarrow \pi^0 X$ . These results are consistent with previous measurements of  $\alpha_{\pi^\pm}$  in our  $p_T$  range.<sup>1,5</sup>

The  $\pi^0$  cross sections agree to within 20% with the pBe  $\rightarrow \pi^\pm X$  data of Ref. 1, when the latter are averaged over  $\pi^+$  and  $\pi^-$  production; our results are also consistent with other measurements<sup>6</sup> of  $\pi^0$  production on C, Be, and hydrogen at 200 GeV/c.

Within experimental errors, the  $\pi^0$  and  $\eta$  cross sections have the same  $p_T$  dependence. The ratio of  $\eta$  to  $\pi^0$  production averaged over our data on carbon is  $\eta/\pi^0 = 0.53 \pm 0.03$ , which is consistent with recent measurements at large  $p_T$  on hydrogen<sup>7</sup> and on beryllium<sup>8</sup> at 200 GeV/c.

One of the earliest indications that large- $p_T$  production could be related to hard scattering of constituents was provided by Donaldson *et al.*,<sup>6</sup> in their observation of an increased yield of  $\pi^0$ 's at large  $p_T$  in  $\pi^+p$  relative to  $pp$  collisions. This

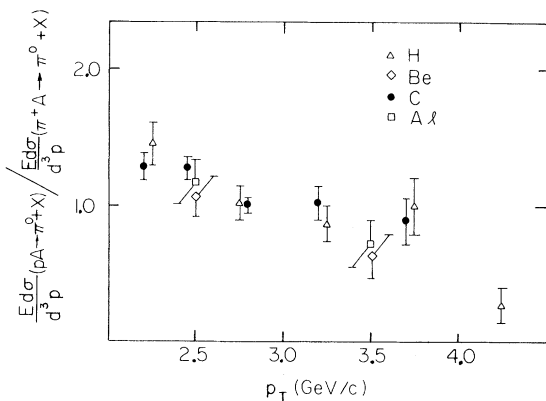


FIG. 3. Ratio of the invariant cross sections for  $\pi^0$  production at 200 GeV/c. The hydrogen data are from Donaldson *et al.*, Ref. 6.

increase was attributed to the higher probability of finding a large- $x$  valence quark in the structure function of a pion. Our results shown in Fig. 3 indicate a similar effect in interactions on nuclear targets. This suggests that any rescattering that occurs in meson production from nuclear targets (i.e.,  $\alpha > 1$ ) does not obscure the differences observed in the hard interactions of pions and protons on hydrogen.

We have, in addition, observed a small signal for  $\omega^0$  production in the decay mode  $\omega^0 \rightarrow \pi^0 \gamma$  ( $30 \pm 10$  events), which corresponds to a cross section  $E d\sigma(pC \rightarrow \omega^0 X)/d^3p$  of  $1.1 \pm 0.4 \mu\text{b}/\text{GeV}^2$  at  $p_T = 2.5 \text{ GeV}/c$  ( $y_{\text{c.m.}} = 0$ ). Thus the ratio of  $\omega^0$  to  $\pi^0$  production is  $\omega^0/\pi^0 = 0.40 \pm 0.13$ , which agrees with a similar measurement<sup>9</sup> made on beryllium. We also quote an upper limit for  $E d\sigma(pC \rightarrow \eta' X)/d^3p$  of  $1.8 \mu\text{b}/\text{GeV}^2$  at  $p_T = 2.5 \text{ GeV}/c$ .

Summarizing our results, we find that the character of the increased production of large- $p_T$   $\pi^0$  and  $\eta$  mesons in the interaction of  $\pi^+$  and protons on nuclear targets is similar to meson production on hydrogen. This suggests a common primary and secondary scattering mechanism for  $\pi^+$ ,  $\pi^0$ , and  $\eta$  production.

<sup>(a)</sup>Permanent address: Texas A & M University, College Station, Tex. 77843.

<sup>(b)</sup>Permanent address: Institute of High Energy Physics, Academia Sinica, P. O. Box 918, People's Republic of China.

<sup>(c)</sup>Present address: University of Arizona, Tucson, Ariz. 85721.

<sup>(d)</sup>Present address: Pennsylvania State University, State College, Pa. 16802.

<sup>1</sup>J. W. Cronin *et al.*, Phys. Rev. D **11**, 3105 (1975); D. Antreasyan *et al.*, Phys. Rev. D **19**, 764 (1979).

<sup>2</sup>J. Pumplin and E. Yen, Phys. Rev. D **11**, 1812 (1975); G. R. Farrar, Phys. Lett. **56B**, 185 (1975); J. H. Kuhn, Phys. Rev. D **13**, 2948 (1976); A. Krzywicki, Phys. Rev. D **14**, 152 (1976); A. Krzywicki, J. Engels, B. Peterson, and U. Sukhatme, Phys. Lett. **85B**, 407 (1979).

<sup>3</sup>C. A. Nelson *et al.*, Fermilab Report No. 82/41, 1982 (to be published).

<sup>4</sup>We also imposed a directionality and timing criterion on the most energetic photon in an event. The effect of these requirements, discussed in Ref. 3 and in the following Letter [M. McLaughlin *et al.*, Phys. Rev. Lett. **51**, 971 (1983)], was crucial for selecting direct photons, but relatively unimportant for  $\pi^0$  and  $\eta$  selection.

<sup>5</sup>C. Bromberg *et al.*, Phys. Rev. Lett. **42**, 1202 (1979); H. J. Frisch *et al.*, Phys. Rev. D **27**, 1001 (1983).

<sup>6</sup>D. C. Carey *et al.*, Phys. Rev. Lett. **33**, 327 (1974); J. A. Appel, *et al.*, Phys. Rev. Lett. **33**, 719 (1974); G. Donaldson *et al.*, Phys. Rev. Lett. **36**, 1110 (1976); R. M. Baltrusaitis *et al.*, Phys. Rev. Lett. **44**, 122 (1980).

<sup>7</sup>G. Donaldson *et al.*, Phys. Rev. Lett. **40**, 684 (1978).

<sup>8</sup>R. M. Baltrusaitis *et al.*, Phys. Lett. **88B**, 372 (1979).

<sup>9</sup>G. Donaldson *et al.*, Phys. Rev. D **21**, 828 (1980).